

Understanding the Adsorption of Rare-Earth Elements in Oligo-Grafted Mesoporous Carbon

P. Gismondi, S. Khalid

To be published in "Langmuir"

December 2021

Photon Sciences

Brookhaven National Laboratory

U.S. Department of Energy

USDOE Office of Science (SC), Basic Energy Sciences (BES) (SC-22)

Notice: This manuscript has been authored by employees of Brookhaven Science Associates, LLC under Contract No. DE-SC0012704 with the U.S. Department of Energy. The publisher by accepting the manuscript for publication acknowledges that the United States Government retains a non-exclusive, paid-up, irrevocable, world-wide license to publish or reproduce the published form of this manuscript, or allow others to do so, for United States Government purposes.

DISCLAIMER

This report was prepared as an account of work sponsored by an agency of the United States Government. Neither the United States Government nor any agency thereof, nor any of their employees, nor any of their contractors, subcontractors, or their employees, makes any warranty, express or implied, or assumes any legal liability or responsibility for the accuracy, completeness, or any third party's use or the results of such use of any information, apparatus, product, or process disclosed, or represents that its use would not infringe privately owned rights. Reference herein to any specific commercial product, process, or service by trade name, trademark, manufacturer, or otherwise, does not necessarily constitute or imply its endorsement, recommendation, or favoring by the United States Government or any agency thereof or its contractors or subcontractors. The views and opinions of authors expressed herein do not necessarily state or reflect those of the United States Government or any agency thereof.

Understanding Adsorption of Rare Earth Elements in Oligo-Grafted Mesoporous Carbon

Pasquale Gismondi¹, Alexei Kuzmin², Colin Unsworth¹, Sylvie Rangan³, Syed Khalid⁴,
Dipendu Saha^{1,*}

- 1.** Chemical Engineering Department, Widener University, 1 University Place, PA 19013, USA
- 2.** Institute of Solid State Physics, University of Latvia, Kengaraga street 8, LV-1063, Riga, Latvia
- 3.** Department of Physics and Astronomy and Laboratory for Surface Modification, Rutgers University, 136 Frelinghuysen Road, Piscataway, New Jersey 08854, USA
- 4.** NSLS-II, Brookhaven National Laboratory, Rochester Ave, Upton, NY 11973

*Corresponding author: D. Saha, E mail: dsaha@widener.edu, Phone: +1 610 499 4056, Fax, +1 610 499 4059

Abstract

Rare earth elements (REEs) are 17 elements of the periodic table primarily consisting of lanthanides. In modern society, the usages of REEs are ubiquitous in almost all modern gadgets and therefore an efficient recovery and separation of REEs are of high importance. Selective adsorption and chelation of REEs in solid sorbents is a unique and sustainable process for their recovery. In this work, single-stranded oligos with 100 units of thymine were grafted on carboxylated mesoporous carbon to synthesize the sorbent with phosphorous and oxygen functionalities. The sorbent was characterized by x-ray photoelectron spectroscopy (XPS), FTIR, and SEM-EDX. Three different REEs with varying atomic radii and density, Lu, Dy, and La were adsorbed onto the carbon from aqueous solutions. It was observed that the adsorbed amounts increased with the increase in atomic radius or decreased atomic density. Calculation of the distribution coefficients for all the equilibrium adsorption amounts suggested that adsorption is more effective in the lower concentration region. The L₃-edge X-ray absorption near edge structure (XANES) confirmed a 3+ oxidation state of REEs in the adsorbed phase. Extended X-ray absorption fine structure (EXAFS) confirmed the binding of REEs with oxygen functionalities in the adsorbed phase. The radial distribution functions (RDF) calculated from the EXAFS data suggest a longer RE-O distance for La compared to that for Lu and Dy. The coordination numbers and Debye-Waller factors have typical values of about 8-9 atoms and 0.01-0.02 Å², respectively.

1. Introduction

Rare earth elements (REEs), often termed Rare Earth Metals (REMs), are seventeen elements of the periodic table including fifteen lanthanides, scandium (Sc), and yttrium (Y). With varying demands, supplies, and utilization, REEs can often be classified into lighter and heavier rare earths¹. Lighter REEs include the lanthanides from lanthanum (La) to samarium (Sm), whereas heavier REEs include the elements from europium (Eu) to lutetium (Lu) and yttrium (Y). Heavier REEs are relatively costlier and scarcer. In modern society, REEs are omnipresent in various items. Different types of REEs are heavily utilized in all types of electronic gadgets, power sources, optical devices, phosphors, and many military applications². Neodymium (Nd) and dysprosium (Dy) are used to produce the world's strongest permanent magnet, whereas Y, Ce, La, Gd, Lu, and Nd are used in manufacture different types of sensors, fiber optics, optical devices, camera lenses, and different other electrical accessories, like resistors and capacitors³. Four rare-earth metals, including Ce, La, Nd, and Y, together contribute to 85% of the world's rare earth element production². Because of its high overspread usages and performance, the global demand for Nd may increase to more than 700% in the next two decades⁴. A part of the REEs play a major role in different energy sectors of the United States and they have been named as energy-critical elements (ECEs). The unavailability of such elements may limit the industrial and scientific sectors of the U.S.⁵

Rare earth elements demonstrate very similar properties with each other and with many other elements of the periodic table and therefore, it is very difficult to separate them. In order to extract the REEs from their ores, usually, solvent extract technique is employed^{6,7,8,9,10,11}. From a global perspective, foreign countries are the lead producers of

REEs that control over 90% of the whole world's REE supply. Recently, a strict export restriction of REE from foreign countries created a shortage of REEs worldwide¹². To maintain a steady supply, recycling and recovering the REEs from non-conventional sources, like fly ash, acid mine drain drainage or 'end-of-life' REE-bearing gadgets may be the feasible strategy. Solvent extraction, despite being used on a large scale, is not effective to recover REEs in small amounts, like that present in the non-conventional sources. Additionally, solvent extraction is very hazardous due to the employment of a large volume of toxic solvents¹³. In addition, it is also time-consuming, labor-intensive^{14,15,16} and leaves toxic residues that are hazardous for disposal.

The adsorption-based process may be suitable alternatives over solvent extraction as it is sustainable, benign, and inexpensive. In addition to pure physisorption, chelation-based binding of REEs onto different types of sorbents has gained attention, especially, the presence of oxygen and phosphorous functionalities have facilitated REE adsorption. Phosphorous-based silica¹⁷ and different types of DNA-hybridized sorbents^{18,19} have been utilized in the successful adsorption of different REEs. *In-situ* L₃-edge extended x-ray absorption fine structure (EXAFS) analysis confirmed the binding of REEs with P and O-functionalities of the sorbent surface. The cell walls of different types of bacterial strains have also been utilized in REE adsorption owing to their rich phosphorus contents^{20,21}. mesoporous silica-based adsorbents grafted with different types of oxygen-bearing chelating agents, like bidentate phthaloyl diamide²² or phenylenedioxy diamide (PDDA)²³ have been successfully utilized in REE separation. In our previous work, we have also demonstrated that different REEs, including Nd and Dy, can be adsorbed in phosphorous

functionalized activated carbon³ and DNA-grafted mesoporous carbon. Our XANES analysis confirmed that the oxidation state did not alter in the DNA grafted carbon and EXAFS confirmed the binding of Nd with O and P-functionalities²⁴.

In this study, we have grafted a singled stranded oligo consisting of 100 thymine units and amino C6 linker on the carboxylated mesoporous carbon synthesized by a soft-templating approach. The reason for choosing mesoporous carbon is that the large (meso) pores will facilitate both grafting and transport of oligos in the course of synthesis. In narrower pores, the diffusion of oligo will be very sluggish resulting in very long time to complete the synthesis process. In addition, a large oligo may block the narrower pore and hence the REE cannot enter the pore and come in contact with the oligos. Thymine unit was chosen as it does not have a primary amine group and hence only primary amine present on the amino C6 linker may react with the carboxylate group of the mesoporous carbon. Three pre-selected REE atoms with varying atomic size and density, lutetium (Lu), dysprosium (Dy), and lanthanum (La) were adsorbed onto the carbon. *In-situ* X-ray absorption spectra (XAS) and radial distribution function (RDF) were employed to understand the binding of those REE atoms with functionalities present on the carbon.

2. Experimental

2.1 Synthesis and functionalization of mesoporous carbon

The synthesis protocol of mesoporous carbon has been obtained from our previous publications^{25,26,27}. Typically, 5.0 g resorcinol as carbon precursor and 4.0 g Pluronic F127 as porogen are dissolved in a 25 mL 1:1 (v/v) mixture of DI water and ethanol. After that, 0.5 mL 36% HCl is to the mixture and stirred overnight. Then 5 mL 37% formaldehyde is added

to the mixture and stirred overnight. After that, the sticky polymer is sprayed on a Petri dish and aged for three days. After that, the polymer is taken out from the petri dish, put in a porcelain boat, and inserted into the Lindberg-Blue tube furnace for carbonization. The furnace is first heated to 100 °C at the ramp rate of 10 °C/min followed by heating to 400 °C at the ramp rate of 2 °C/min and then finally to 900 °C at the ramp rate of 10 °C/min. After the heating profile, the furnace is cooled to room temperature. All the heating and cooling operations are performed in nitrogen flow. Upon cooling, the porcelain boat is taken out and the resultant mesoporous carbon ground in a coffee grinder.

In order to functionalize the mesoporous carbon with the carboxylate group, at first, a 50 mL 3:1 mixture of concentrated H₂SO₄ and concentrated HNO₃ was prepared in a round-bottom flask and heated to 65 °C in a silicone oil bath. After that, 1 g mesoporous carbon is added to the heated acid mixture and stirred vigorously for 7 hours. Then, the acid mixture is cooled, quenched in ice-cold water, and washed with DI water repeatedly. Finally, it is filtered and dried in a muffle furnace.

2.2 Grafting of oligo on carboxylated mesoporous carbon

At first, 100 mg carboxylated mesoporous carbon is dispersed in 250 mL DI water under vigorous stirring. After that, aqueous solutions of 50 mL 500 mM MES (2-(*N*-morpholino) ethanesulfonic acid) buffer and 115 mL of 50 mg/mL *N*-hydroxy succinimide were added to the mixture under stirring. Then, a freshly prepared aqueous solution of 60 mL 10mg/mL EDC (1-Ethyl-3-(3-dimethylaminopropyl) carbodiimide) was added to the same mixture and stirred for 30 minutes. In the end, the mesoporous carbon was allowed to

settle, the solution was decanted and the carbon was washed three times with 50 mL MES solution. After that, the mesoporous carbon was filtered out and redispersed in 2 mL oligo solution (100 units of thymine with amino C6 linker in 5' end and PO₄⁻ in the 3' end) with 1 mL 50 mL MES buffer. The suspension was stirred for an hour and then frozen in a refrigerator at -20 °C overnight. After that, the suspension was thawed, washed with DI water 3 times, filtered, dried, and stored in -20 °C. The overall schematic of oligo grafting process is shown in [figure 1](#).

2.3 Characterization of oligo grafted mesoporous carbon

As we cannot outgas and measure the porosity of the oligo-grafted mesoporous carbon (as long exposure/heat treatment may degrade the oligo), we measured the porosity of the pristine mesoporous carbon only. The porosity, including Brunauer-Emmett-Teller (BET) specific surface area and pore volume, was calculated by analyzing N₂ adsorption-desorption at 77 K for larger pore widths and CO₂ adsorption at 273 K for narrower pore widths. Fourier-transform infrared (FTIR) spectra of pristine, carboxylated and oligo-grafted mesoporous carbon were measured using Nicolet® Avatar FT-IR Spectrometer in ATR mode and averaged over 30 scans. The SEM-EDX images were obtained in the JEOL 7500F HRSEM instrument with 15 kV potential. The TEM image was obtained in Carl Zeiss Libra 120 TEM operating at 80 kV. The X-ray photoelectron spectroscopy (XPS) data were obtained in the Thermo-Fisher K-alpha instrument using an *AlKα* x-ray source (1486.7 eV) with an overall resolution of 0.7 eV. In the course of the experiment, the charge compensation was performed by using a combination of low-energy electrons and ions.

2.4 Adsorption of rare-earth elements

In order to perform the adsorption of rare earth elements in the aqueous phase, 10, 100, 300, and 500 ppm of Lu, Dy, and La solution was made from $\text{Lu}(\text{NO}_3)_3$, $\text{Dy}(\text{NO}_3)_3$, and $\text{La}(\text{NO}_3)_3$, respectively. In the course adsorption, 25 mg oligo-grafted mesoporous carbon was added to 25 mL of rare earth solution and stirred for 4 hours. After that, the carbon is filtered out, and the solution is preserved. The concentration of REE was measured by ICP-MS and the amount adsorbed was calculated by difference. All the experiments were performed in duplicate and the average values were reported along with standard deviation as error bars. ICP-MS, using 10 ppb Sn with m/z number of 118 (sigma 96215) as an internal standard as it is compatible and has limited interference to all REEs. A trial has been done before formal analysis and the stability ratio of Sn-118 ranges from 90-120%. The test with a ratio below 90% or higher than 120% will be excluded and rerun.

2.5 Measurement of x-ray absorption (XAS) spectroscopy

The binding nature of rare earth elements with oligo-grafted mesoporous carbon was investigated by x-ray absorption spectroscopy (XAS); X-ray absorption near edge structure (XANES) and Extended X-ray Absorption Fine Structure (EXAFS). 0.2 g oligo-grafted mesoporous carbon was added to 250 mL of a 1000 ppm solution of each of Lu, Dy, and La, and the suspension was stirred for 4 hours. After that, the carbon was separated by filtration, dried, and preserved for XAS analysis. X-ray absorption spectra of Lu, Dy, and La adsorbed on carbon along with pristine $\text{Lu}(\text{NO}_3)_3$, $\text{Dy}(\text{NO}_3)_3$, and $\text{La}(\text{NO}_3)_3$ were recorded at National Synchrotron Light Source II (NSLS-II) beamline QAS of Brookhaven National Laboratory (BNL). All the XAS measurements were performed at room temperature. X-ray absorption

spectra (XAS) of La, Dy, and Lu rare-earth (RE) ions absorbed on oligo-grafted mesoporous carbon (PC) and reference REE-nitrates were recorded in fluorescence and transmission modes, respectively, at the RE L₃-edges. The synchrotron x-ray radiation was monochromatized using double-crystal Si(111) monochromator, which was 40% detuned to eliminate higher harmonics, mostly the third one (as the second one is almost eliminated by the virtue of the crystal). The intensity of the x-rays before the sample was measured using an ion chamber. The XAS of reference compounds (REE nitrates) were collected in the transmission mode, whereas the XAS of RE ions in PC samples were recorded in the fluorescence mode. In the transmission mode, an ion chamber located behind the sample was used as the second detector, whereas in the fluorescence mode, PIPS (Passivated Implanted Planar Silicon) large diode detector was employed. The energy scale of the monochromator was calibrated using chromium foil. To improve statistics, the average spectrum over nine experimental measurements was used in the analysis of RE ions in PC samples. The X-ray absorption near edge structure (XANES) and extended X-ray absorption fine structure (EXAFS) parts of the XAS spectra were extracted using a conventional procedure. The relatively low signal-to-noise ratio of the experimental data for RE ions in PC, especially for La, did not allow us to perform their comprehensive analysis, however, we were able to evaluate the values of the mean RE-O distances and to estimate coordination numbers and Debye-Waller factors for the first coordination shell of REEs.

3. Results and Discussion

3.1 Materials Characteristics

Fourier transform infrared spectra (FTIR) of pristine, carboxylated and oligo-grafted carbons are shown in [figure 2](#). For carboxylated carbon, the weak peak at around 1744 cm^{-1} and a sharp peak around 1575 cm^{-1} signify the C=O stretch of the carboxylic group²⁸. In DNA grafted carbons, the peak at 1744 cm^{-1} is slightly shifted to a lower wavelength ($\sim 1731\text{ cm}^{-1}$) that may be attributed to the possible formation of an amide bond between oligo and carboxylate group or the presence of a similar bond in the thymine base of oligo. Due to the presence of strong absorption peaks in the carboxylated carbons, it was not feasible to distinctly identify the peaks associated with oligo strands in the DNA functionalized carbons. However, the few peaks around 1366 , 1200 , and 1131 cm^{-1} may be associated with the antisymmetric stretching of phosphate groups²⁹.

The total elemental composition of the DNA grafted carbon, as obtained by x-ray photoelectron spectroscopy (XPS) is shown in [table 1](#) and the peak fitting results of N-1s, O-1s and P-2p core levels are shown in [figure 3](#).

Table 1: Elemental composition of DNA-grafted carbon

Elemental composition	
P	0.7 %
O	15.0 %
S	0.3 %
F	0.5 %
C	80.1 %
N	3.6 %

The total N, P and O contents are 3.6, 0.7, and 15.0 at.%, respectively, and part of those are attributed to the oligo strand. In the P-2p core level spectrum, the doublet centered at 134 eV is unambiguously attributed to the phosphate group of oligo. For O 1s and N 1s, the peak fitting indicates that the components expected for the oligo are present (in red), but are also accompanied by other species (in black). The oligo peaks intensities are fitted using the expected N/P ratio of 2 and O/P ratio of 8. For O-1s, the peaks at 531.4 and 532.7 eV are associated with the base/sugar and phosphate component of the oligo, respectively. For N-1s, it is possible to fit a peak at 400.4 eV associated with the thymine base of the oligo. Three other components at 400.4 eV, 402.3 eV and 398.6 eV may be attributed to additional N in an environment similar to the oligo, and to the -NH^{3+} and conjugated -N= functionalities, respectively. The additional amounts of nitrogen may be attributed to the unreacted EDC or part of the MES buffer left in the system. The presence of sulfur in the system corroborates the possible presence of MES. Excess oxygen indicates that the mesoporous carbon itself contains a large fraction of oxygen as well, as expected for air exposed samples. The SEM-EDX mapping of the C, N, O, S, and P are shown in [figure 4 \(a-f\)](#). It shows that the elements are quite uniformly distributed throughout the carbon matrix. The TEM image of the mesoporous carbon are shown in [figure S2 \(a, b\)](#) of the supporting information.

The N_2 adsorption-desorption plot of pristine mesoporous carbon at 77K ([figure S1](#), supporting information) suggested a type IV isotherm according to the IUPAC classification, which also bears the fingerprint mesoporosity. The pore size distribution of pristine mesoporous carbon, suggests that it had the mesopore width of 48 Å along with a few micropores. The BET specific surface area of was 605 m^2/g . We could not measure the

porosity after oligo grafting as it could not be outgassed at elevated temperature and hence the trapped water molecules could not be removed prior to N₂ adsorption.

3.2 Adsorption of rare elements

The adsorption data of Lu, Dy, and La are shown in [figure 5\(a\)](#) as bar plots for the initial concentrations of 10, 100, 300, and 500 ppm. As expected, the adsorbed amounts of REEs increase with the increase in initial concentration from 10 to 500 ppm. At 500 ppm, the adsorbed amounts of Lu, Dy, and La are in 9.57, 38.27, and 52.15 mg/g, respectively. In addition, it is also observed that adsorbed amount followed the trend of Lu<Dy<La. It essentially suggests that adsorbed amount increases with the increase in atomic radius (Lu= 173 pm; Dy= 178 pm; La= 187 pm)²⁴. This effect has been further elaborated in [figure 5\(c\)](#). It demonstrates that adsorbed amounts increase within the atomic radius for all the concentrations. This trend is in line with our previous work²⁴. In addition, it has also been noticed that amounts decrease with an increase in the density (Lu³⁰= 9.7 g/cm³; Dy³¹= 8.6 g/cm³; La³²= 6.18 g/cm³) as density decreases with the increase in atomic size.

For adsorption in a liquid medium, it is a common practice to calculate the distribution coefficient (K_d) calculated as

$$K_d = \left(\frac{C_i - C_f}{C_f} \right) \left(\frac{V}{m} \right) \quad (1)$$

Where C_i : initial concentration; C_f : final concentration; V : volume of the solution and m : mass of the adsorbent. The plots of the distribution coefficients of Lu, Dy, and La as a function of initial concentration are shown in [figure 5\(b\)](#). The trend of K_d among the three REEs follows the same trend that of adsorption, i.e., Lu<Dy<La. In addition, it is also shown that K_d

decreases with the increase in initial concentration suggesting that adsorption is more effective in the lower concentration^{3,24}. At 10 ppm, the K_d values for Lu, Dy, and La are 917.5, 1343.5, and 1752.5 mL/g, respectively, that change to 19.5, 82.9, and 116.4 mL/g, respectively, at 500 ppm.

3.3 XAS analysis

The EXAFS contributions from the first coordination shells of REEs were isolated in the range of about 0.8-3.0 Å using the Fourier filtering procedure and best-fitted in the k -space using the regularization method³³, which was successfully applied in the past to the study of the RE ion environment in oxide glasses^{34,35}. In this approach, one does not make any assumptions about the shape of the radial distribution function (RDF) $g(R)$, so that analysis can be reliably performed for the case of a strongly disordered or distorted environment. The contribution to the total EXAFS spectrum from the first coordination shell located in the range from R_{min} to R_{max} is given by^{36,37}

$$\chi(k) = S_0^2 \int_{R_{min}}^{R_{max}} g(R) \frac{|f^l(\pi, k, R)|}{kR^2} \sin[2kR + \psi^l(\pi, k, R) + 2\delta_c^l(k)] e^{-2R/\lambda(k)} dR. \quad (2)$$

Here S_0^2 is a many-body reduction factor accounting for amplitude damping due to multi-electron effects (intrinsic losses), $\lambda(k)$ is the energy-dependent mean free path of the photoelectron. The backscattering amplitude $f^l(\pi, k, R)$ and phase shift $\psi^l(\pi, k, R)$ functions account for the photoelectron scattering by the neighboring oxygen atoms, and the final-state phase shift $2\delta_c^l(k)$ is introduced by the absorbing RE atom (l is the orbital momentum of an absorption edge). The last four functions were calculated within the muffin-tin approximation using ab initio self-consistent real-space multiple-scattering FEFF8.50L

code^{38,39}. The calculations were performed for a cluster with a radius of 8 Å representing a fragment of the nitrate structure and centered at the required RE atom. The photoelectron inelastic losses were accounted for within the one-plasmon approximation using the complex exchange-correlation Hedin-Lundqvist potential⁴⁰.

Normalized rare-earth L₃-edge XANES spectra in RE nitrates and oligo-grafted mesoporous carbon (PC) are shown in Fig. 6 (a-c). The positions of the absorption edges coincide well for the three edges suggesting the same (3+) oxidation state of rare-earth ions. All spectra exhibit the so-called “white line” (WL), i.e., a strong absorption resonance located just above the absorption edge. It is due to the electric-dipole allowed ($\Delta l = +1$) transition from the core state $2p_{3/2}(\text{RE})$ to quasi bound states having the $5d(\text{RE})$ atomic character⁴¹. All XANES spectra have close shapes, however, the frequency of the main oscillation above the WL due to the nearest oxygen atoms is slightly smaller for the PC samples than for nitrates, indicating a small difference in the mean RE-O distances. This effect is better visible in the XANES spectra of Dy (at 7820 eV) and Lu (at 9275 eV) samples which have a better signal-to-noise ratio.

The results of the analysis for the first coordination shell EXAFS contribution using the method described above are shown in Fig. 7 (a-f). The model based on the RDF $g(R)$ reproduces well the experimental first-shell EXAFS spectra and their Fourier transforms for all six samples. Note that in each case the k -space range used in the simulations was carefully selected and is limited by the noise present in the experimental data. As a result, we obtained the mean values of the interatomic RE-O distances, which are shown in Fig. 8. One can note

that the distance is always slightly shorter (by 0.03-0.07 Å) in PC samples than in nitrates, supporting our conclusion from the analysis of XANES. Moreover, the mean RE-O distance in samples containing La is much larger (by ~0.2 Å) than in others. Such difference correlates with the well-known RE-O bond length variation throughout the lanthanoid(3+) series due to a decrease of the rare-earth ionic radius^{42,43}. Besides, the difference in the values of the RE-O distances in the PC samples is in good agreement with the difference in the RE(3+) ionic radii proposed by Shannon⁴⁴. Also, the absolute values of the RE-O bond lengths are close to that found for the RE solvated ions^{42,43}.

Unfortunately, the experimental data quality did not allow us to get accurate values of coordination numbers and Debye-Waller factors. However, we were able to estimate their values in all samples to be equal for the coordination numbers of about $N=8-9\pm 1$ and for the Debye-Waller factor of about $\sigma^2\approx 0.01-0.02 \text{ \AA}^2$. These values are typical for the RE(3+) ions coordinated to oxygen atoms.

Conclusions

In this work, we have successfully synthesized oligo-grafted mesoporous carbons with 100 units of thymine. This sorbent was properly characterized with XPS, FTIR and SEM-EDX. The three different REEs with varying sizes and densities, Lu, Dy, and La were adsorbed onto this carbon from their aqueous solutions. It was observed that adsorbed amount increases with the increase in atomic radii or decrease in density. The analysis of the RE L₃-edge X-ray absorption spectra suggests that La, Dy, and Lu ions in oligo-grafted mesoporous carbon are preferentially coordinated by oxygen ions and have a 3+ oxidation state with the

mean interatomic RE-O distances close to that for the solvated RE ions. The mean La-O distance is longer by about 0.2 Å than that of Dy-O and Lu-O due to the difference in the RE ionic radii. The coordination numbers and Debye-Waller factors have typical values of about 8-9 oxygen atoms and $\sigma^2 \approx 0.01-0.02 \text{ \AA}^2$. These results suggested that physical adsorption onto the pores and chelation with the heteroatoms (primarily oxygen) played a role in the uptake of REEs in our sorbent.

Acknowledgements

This work has been funded by National Science Foundation (NSF) with grant number 1837202. P.G. and C. E. U. acknowledge support from the School of Engineering of Widener University. This research used resources of the National Synchrotron Light Source II, a U.S. Department of Energy (DOE) Office of Science User Facility operated for the DOE Office of Science by Brookhaven National Laboratory under Contract No. DE-SC0012704. The authors acknowledge Dr. Jamie Morris of Singh Center of Nanotechnology of the University of Pennsylvania for assisting in SEM-EDX imaging. Institute of Solid State Physics, University of Latvia as the Center of Excellence has received funding from the European Union's Horizon 2020 Framework Programme H2020-WIDESPREAD-01-2016-2017-TeamingPhase2 under grant agreement No. 739508, project CAMART2.

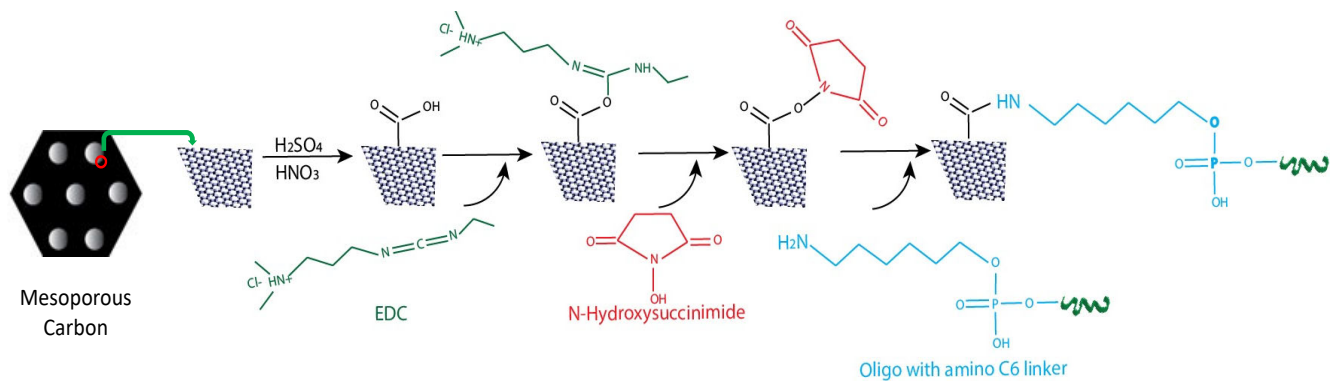


Figure 1. Schematic of grafting procedure of oligo on the pore surface of mesoporous carbon

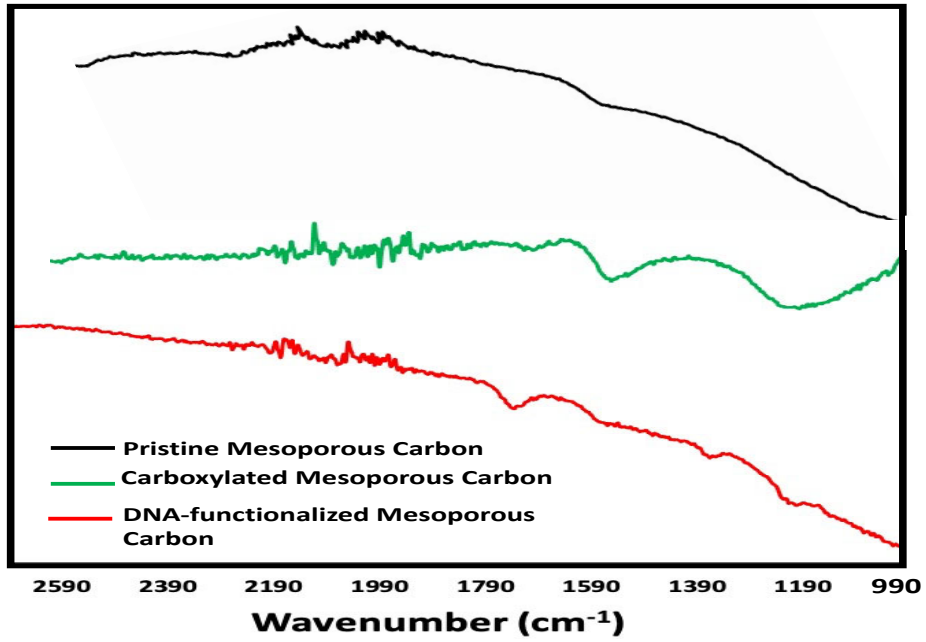


Figure 2. FTIR of pristine, carboxylated and DNA-grafted mesoporous carbon

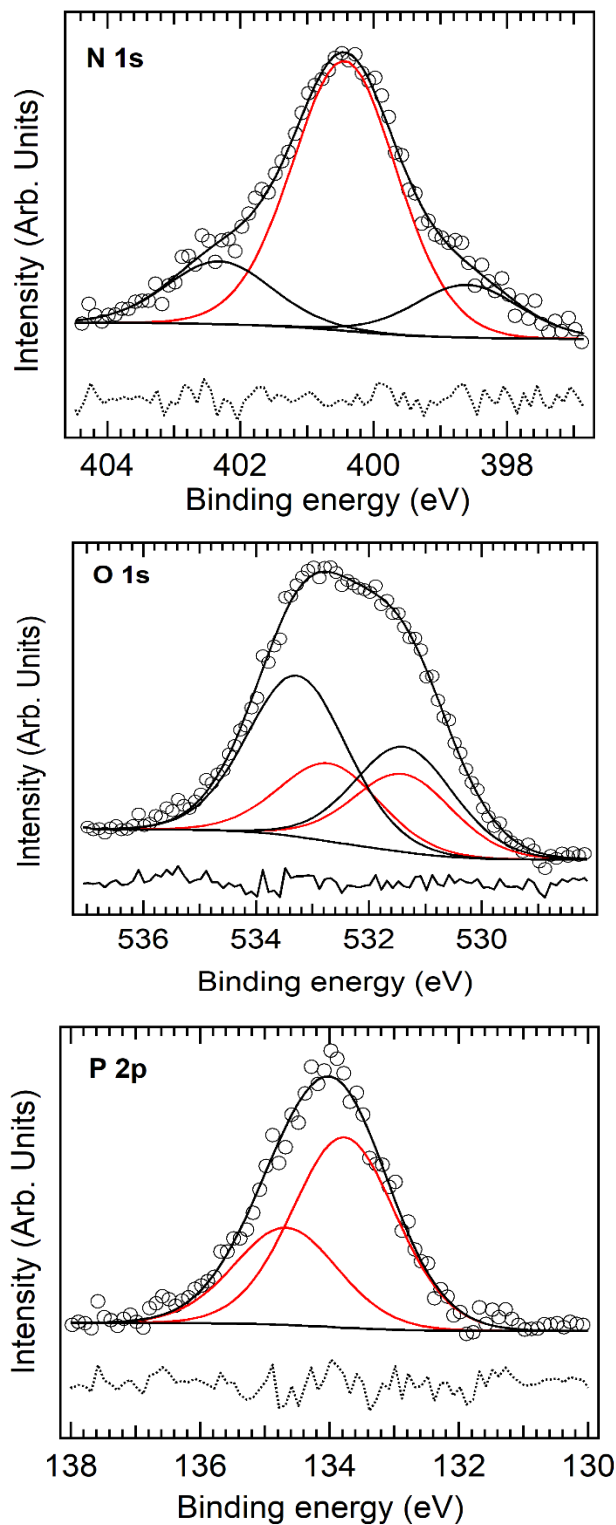


Figure 3. XPS peak fitting results of DNA-grafted carbon for N-1s(a), O-1s (b) and P-2p (c). The red curves indicate the fraction of the fitting attributed to the DNA component only.

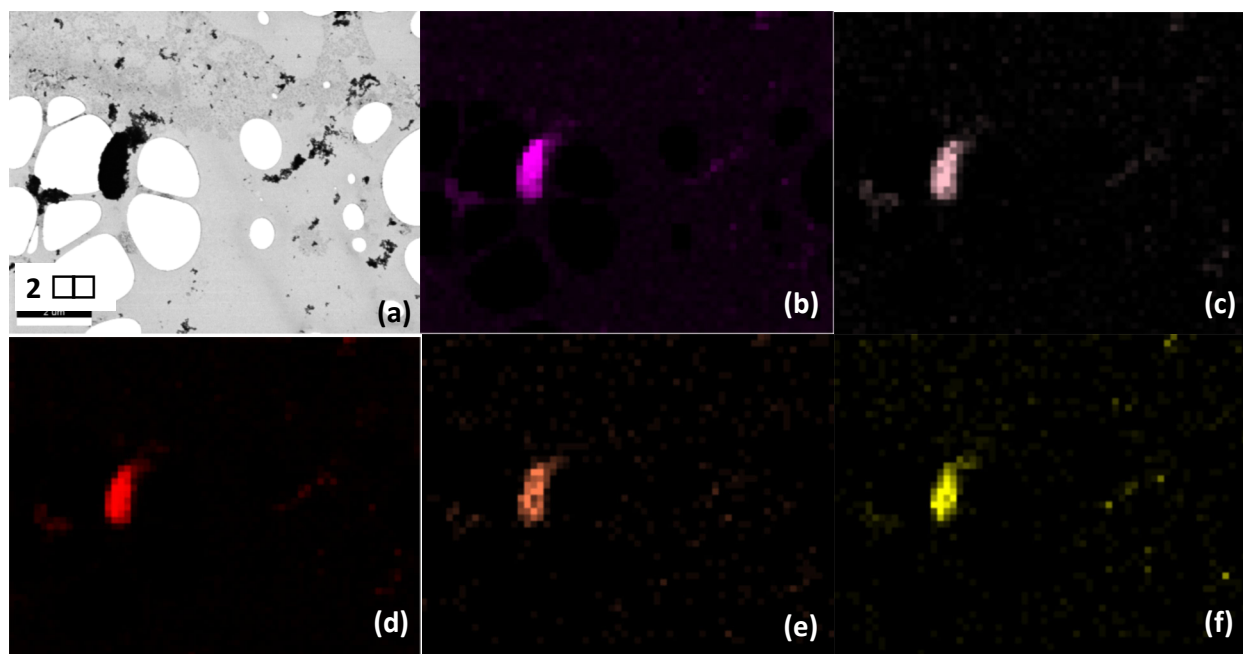


Figure 4. SEM image (a) EDX mapping of the mesoporous carbon, C-1K (b), N-K (c), O-K(d), P-K (e) and S-K (f)

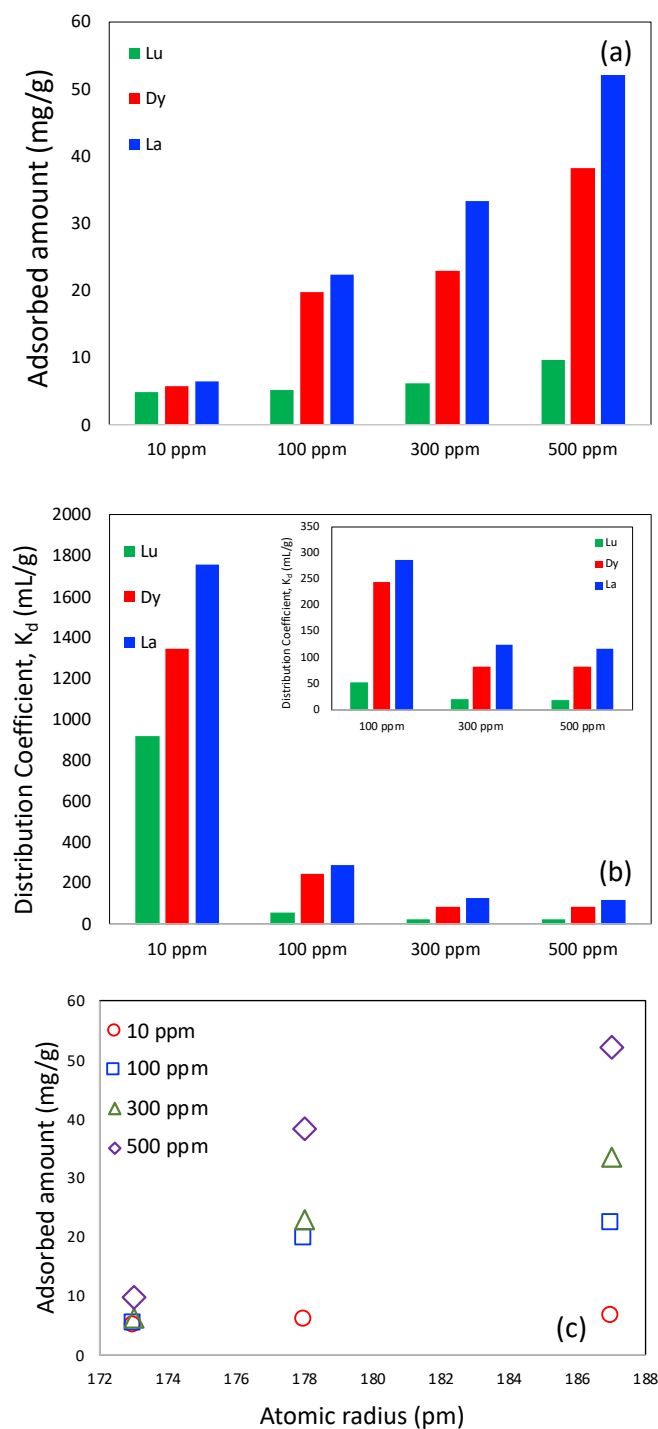


Figure 5. Adsorbed amount (a) and distribution coefficient (K_d) of Lu, Dy and La in oligo-grafted mesoporous carbon and as a function of initial REE concentration (inset of (b) shows the magnified view of the K_d for the initial concentration of 100, 300 and 500 ppm. Adsorbed amounts as a function of atomic radius (c)

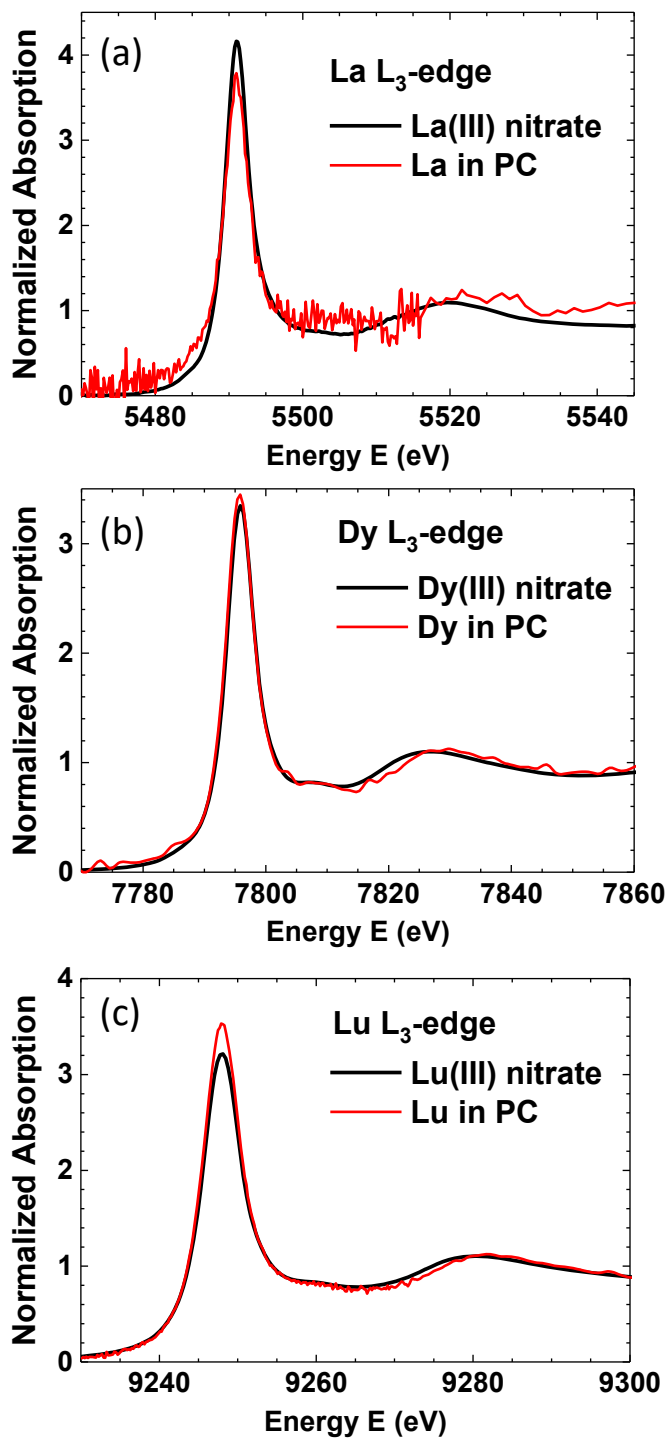


Figure 6. Normalized rare-earth L₃-edge XANES spectra for nitrates and oligo-grafted mesoporous carbon (PC) for La (a), Dy (b) and Lu (c) .

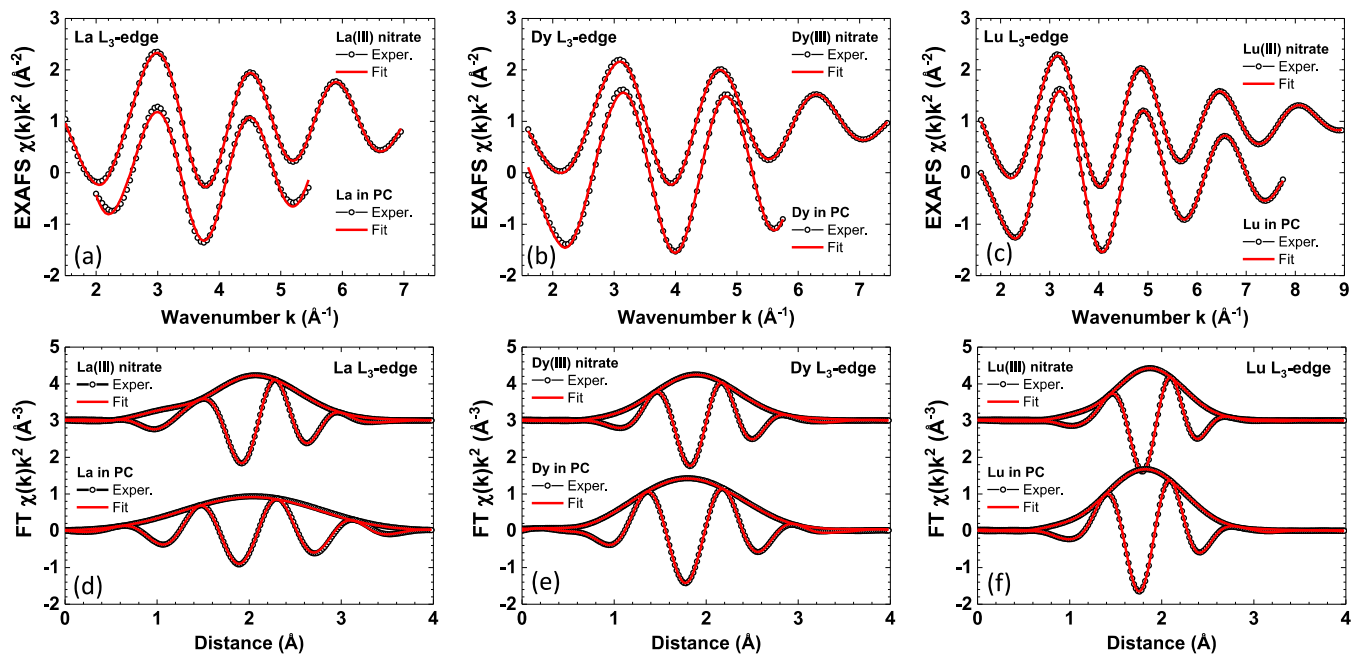


Figure 7. Comparison of the experimental (open circles) and best-fit (solid line) EXAFS spectra $\chi(k)k^2$ (upper row; La (a), Dy (b), Lu (c)) and their Fourier transforms (FTs) (lower row; La (d), Dy (e), Lu (f)) for La, Dy, and Lu ions for nitrates and oligo-grafted mesoporous carbon (PC).

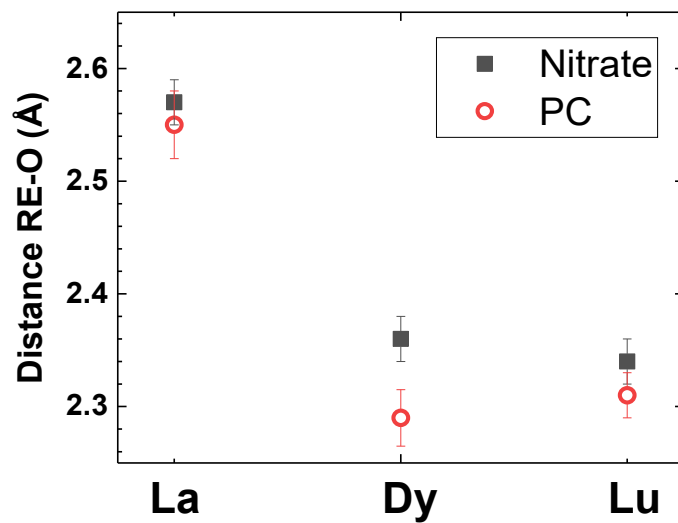


Figure 8. Values of the mean RE-O distances in nitrates (solid squares) and oligo-grafted mesoporous carbon (PC) (open circles).

References

- ¹ Anastopoulou, A. Bhatnagar, E. C. Limac, Adsorption Of Rare Earth Metals: A Review of Recent Literature. *J. Molecular Liquids*. 2016, 221, 954-962.
- ² N. Das, D. Das, Recovery Of Rare Earth Metals Through Biosorption: An Overview. *J. Rare Earths*. 2013, 31, 933-943.
- ³ D. Saha, S.D. Akkoyunlu, R. Thorpe, D.K. Hensley, J. Chen, Adsorptive recovery of neodymium and dysprosium in phosphorous functionalized nanoporous carbon. *J. Environmental Chemical Engineering* 2017, 5, 4684-4692.
- ⁴ E. Alonso, A.M. Sherman, T.J. Wallington, M.P. Everson, F.R. Field, R. Roth, R.E. Kirchain, Evaluating Rare Earth Element Availability: A Case with Revolutionary Demand from Clean Technologies. *Environ. Sci. Technol.* 2012, 46, 3406-3414.
- ⁵ <https://www.aps.org/policy/reports/popa-reports/upload/elementsreport.pdf> (accessed in Jan 2017)
- ⁶ Sengupta, J. G.; Determination of Scandium, Yttrium and Lanthanides in Silicate Rocks and Four New Canadian Iron Formation Reference Materials by Flame Atomic-Absorption Spectrometry with Micro Sample Injection. *Talanta*. 1984, 31, 1045-1051.
- ⁷ Kim, J. S.; Lee, C. H.; Han, S. H.; Suh, M. Y. Studies on complexation and solvent extraction of lanthanides in the presence of diaza-18-crown-6-di-isopropionic acid. *Talanta*. 1997, 45, 437-444.
- ⁸ Xiong, C. H.; Liu, X. Z.; Yao, C. P. Effect of pH on sorption for RE(III) and sorption behaviors of Sm(III) by D152 resin. *J. Rare Earths*. 2008, 26, 851-856.
- ⁹ Xiong, C. H. Sorption behavior of D155 resin for Ce(III). *Ind. J. Chem.* 2008, 47A, 1377-1380.
- ¹⁰ Zhu, Y.; Zheng, Y.; Wang, A. A simple approach to fabricate granular adsorbent for adsorption of rare elements. *Int. J. Biol. Macromol.* 2015, 72, 410-420.
- ¹¹ Xie, F; Zhang, T. A.; Dreisinger, D.; Doyle, F. A critical review on solvent extraction of rare earths from aqueous solutions. *Minerals Engg.* 2014, 56, 10-28.
- ¹² Zheng, X.; Liu, E.; Zhang, F.; Yan, Y.; Pan, J. Efficient adsorption and separation of dysprosium from NdFeB magnets in an acidic system by ion imprinted mesoporous silica sealed in a dialysis bag. *Green Chem.* 2016, 18, 5031-5040.
- ¹³ Yao, C. P. Adsorption and desorption properties of D151 resin for Ce(III). *J. Rare Earths*. 2010, 28, 183-188.
- ¹⁴ Ritcey, G. M; Ashbrook, A. W. Solvent Extraction: Principle and Applications to Process Metallurgy, Part I. Amsterdam. *Elsevier Press*. 1984, 603.
- ¹⁵ Samuelson O. Ion Exchangers in Analytical Chemistry. *John Wiley*. 1972, 415.
- ¹⁶ Xiong, C. H.; Zheng, Z. W. Evaluation of D113 cation exchange resin for the removal of Eu(III) from aqueous solution. *J. Rare Earths*. 2010, 28, 862-867.
- ¹⁷ H-J. Park, L. L. Tavlarides, Adsorption of Neodymium(III) from Aqueous Solutions Using a Phosphorus Functionalized Adsorbent, *Ind. Eng. Chem. Res.* 2010, 49, 12567-12575.

-
- ¹⁸ Y. Takahashi, K. Kondo, A. Miyaji, Y. Watanabe, Q. Fan, T. Honma, K. Tanaka, Recovery and Separation of Rare Earth Elements Using Salmon Milt. *Plos One* 2014, 9, e114858.
- ¹⁹ Y. Takahashi, K. Kondo, K. Miyaji, A.M. Umeo, T. Honma, S. Asaoka, Recovery and Separation of Rare Earth Elements Using Columns Loaded with DNA-filter Hybrid. *Analytical sciences*. 2012, 28, 985-992.
- ²⁰ Y. Takahashi, X. Châtellier, K.H. Hattori, K. Kato, D. Fortin, Adsorption of Rare Earth Elements onto Bacterial Cell Walls and Its Implication for REE Sorption onto Natural Microbial Mats. *Chemical Geology*. 2005, 219, 53– 67.
- ²¹ H. Moriwaki, R. Masuda, Y. Yamazaki, K. Horiuchi, M. Miyashita, J. Kasahara, T. Tanaka, H. Yamamoto, Application of Freeze-Dried Powders of Genetically Engineered Microbial Strains as Adsorbents for Rare Earth Metal Ions, *ACS Appl. Mater. Interfaces*. 2016, 8, 26524–26531.
- ²² Y. Hu, E. Drouin, D. Lariviere, F. Kleitz, F-G Fontaine, Highly Efficient and Selective Recovery of Rare Earth Elements Using Mesoporous Silica Functionalized by Preorganized Chelating Ligands. *ACS Appl. Mater. Interfaces* 2017, 9, 38584–38593.
- ²³ Y. Hu, L.C.M. Castro, E. Drouin, J. Florek, H. Kahlig, K. Lariviere. F-G Fontaine, Size-Selective Separation of Rare Earth Elements Using Functionalized Mesoporous Silica Materials. *ACS Appl. Mater. Interfaces* 2019, 11, 23681–23691.
- ²⁴ D. Saha, C.C. Kuo, A. Kuzmin, S. Khalid, D. Saha, Adsorption of Rare Earth Elements onto DNA-Functionalized Mesoporous Carbon. *ACS Appl. Mater. Interfaces* 12, 43180-43190.
- ²⁵ D. Saha, R. Zacharia, A.K. Naskar, Soft-templated Mesoporous Carbons: Chemistry and Characteristics. *Polymer Precursor-Derived Carbon*, Chapter 4, pp 61-83, 2014 (10.1021/bk-2014-1173.ch004).
- ²⁶ D. Saha, C. P. Richards, R. G. Haines, N. D. D'Alessandro, M. J. Kienbaum, C. A. Griffaton, Competitive Adsorption of Lead in Sulfur and Iron Dual-Doped Mesoporous Carbons, *Molecules* 2020, vol. 25 pp 403.
- ²⁷ D. Saha, S. Barakat, S. Van Bramer, K.A. Nelson, D.K. Hensley, J. Chen, Non-competitive and competitive adsorption of heavy metals in sulfur-functionalized ordered mesoporous carbon, *ACS Applied Materials and Interfaces*, 2016, vol. 8 no. 49 pp. 34132–34142.
- ²⁸ M. J. Park, J. K. Lee, B. S. Lee, Y-W.n Lee, I. S. Choi, S-G. Lee, Covalent Modification of Multiwalled Carbon Nanotubes with Imidazolium-Based Ionic Liquids: Effect of Anions on Solubility, *Chem. Mater*. 2006, 18, 1546-1551.
- ²⁹ J.J. van den Beucken, M.R. Vos, P.C. Thune, T. Hayakawa, T. Fukushima, Y. Okahata, X.F. Walboomers, N.A. Sommerdijk, R.J. Nolte, J.A. Jansen, Fabrication, characterization, and biological assessment of multilayered DNA- coatings for biomaterial purposes, *Biomaterials* 27 (2006) 691–701.
- ³⁰ <https://www.lenntech.com/periodic/elements/lu.htm> (Accessed August 2021)
- ³¹ <https://www.lenntech.com/periodic/elements/dy.htm> (Accessed August 2021)
- ³² <https://www.lenntech.com/periodic/elements/la.htm> (Accessed August 2021)

-
- ³³ A. Kuzmin and J. Purans, Dehydration of the molybdenum trioxide hydrates $\text{MoO}_3 \cdot n\text{H}_2\text{O}$: in situ x-ray absorption spectroscopy study at the Mo K edge, *J. Phys.: Condensed Matter* 2000, 12, 1959-1970.
- ³⁴ F. Rocca, A. Dalmaso, F. Monti, A. Kuzmin, D. Pasqualini, EXAFS study of Tb-doped silica xerogels, *J. Synchrotron Rad.* 1999, 6, 737-739.
- ³⁵ F. Rocca, G. Dalba, R. Grisenti, M. Bettinelli, F. Monti, A. Kuzmin, Extended X-ray absorption fine structure measurements of the local environment of Pr^{3+} ions in silica xerogels and zinc borate glasses, *J. Non-Cryst. Solids* 1998, 232-234, 581-586.
- ³⁶ E.A. Stern, D.E. Sayers, F.W. Lytle, Extended x-ray-absorption fine-structure technique. III. Determination of physical parameters, *Phys. Rev. B* 1975, 11, 4836-4846.
- ³⁷ P.A. Lee, P.H. Citrin, P. Eisenberger, B.M. Kincaid, Extended x-ray absorption fine structure—its strengths and limitations as a structural tool, *Rev. Mod. Phys.* 1981, 53, 769-806.
- ³⁸ A.L. Ankudinov, B. Ravel, J.J. Rehr, S.D. Conradson, Real-Space Multiple-Scattering Calculation and Interpretation of X-Ray-Absorption Near-Edge Structure, *Phys. Rev. B* 1998, 58, 7565-7576.
- ³⁹ J.J. Rehr and R.C. Albers, Theoretical Approaches to X-Ray Absorption Fine Structure, *Rev. Mod. Phys.* 2000, 72, 621-654.
- ⁴⁰ L. Hedin and S. Lundqvist, Explicit local exchange-correlation potentials, *J. Phys. C: Solid State Phys.* 1971, 4, 2064-2083.
- ⁴¹ F. Rocca, A. Kuzmin, J. Purans, G. Mariotto, X-ray absorption spectroscopy study of a Nd^{3+} -exchanged β "-alumina crystal, *Phys. Rev. B* 1994, 50, 6662-6672.
- ⁴² S. Ishiguro, Y. Umebayashi, K. Kato, R. Takahashi, K. Ozutsumi, Strong and weak solvation steric effects on lanthanoid(III) ions in N,N-dimethylformamide—N,N-dimethylacetamide mixtures, *J. Chem. Soc., Faraday Trans.* 1998, 94, 3607-3612.
- ⁴³ I. Persson, P. D'Angelo, S. De Panfilis, M. Sandstrom, L. Eriksson, Hydration of Lanthanoid(III) Ions in Aqueous Solution and Crystalline Hydrates Studied by EXAFS Spectroscopy and Crystallography: The Myth of the "Gadolinium Break", *Chem. Eur. J.* 2008, 14, 3056-3066.
- ⁴⁴ R. D. Shannon, Revised Effective Ionic Radii and Systematic Studies of Interatomic Distances in Halides and Chalcogenides, *Acta Cryst.* 1976, A32, 751-767.

TOC Graphic

